



Dimeric iron(III) complexes with salicylaldehyde ligands: structures, magnetic properties, and activity of H₂O₂ disproportionation

Wei-Hsian Chen^a, Ho-Hsiang Wei^{a,*}, Gene-Hsiang Lee^b, Yu Wang^b

^a Department of Chemistry, TamKang University, Tamsui, Taiwan, ROC

^b Instrumentation Center of College of Science, National Taiwan University, Taipei, Taiwan, ROC

Received 11 August 2000; accepted 7 November 2000

Abstract

The preparations, characterizations, structures, magnetic properties and catalase-like activities of four new alkoxy bridged dimeric five-coordinate iron(III) salicylaldehyde complexes, [FeL¹Cl]₂ (**1**) (H₂L¹ = *N*-(3-hydroxypropyl)(5-bromosalicylaldehyde)), [FeL²Cl]₂ (**2**) (H₂L² = *N*-(3-hydroxypropyl)(3-methoxysalicylaldehyde)), [FeL³Cl]₂ (**3**) (H₂L³ = *N*-(3-hydroxypropyl)(4-diethylaminosalicylaldehyde)), and [FeL⁴Cl]₂ (**4**) (H₂L⁴ = *N*-(3-hydroxypropyl)(3,5-diiodosalicylaldehyde)) are reported. The crystal structure of complexes **1–3** show an alkoxy bridged dimeric iron(III) complex, which occupies a site of inversion symmetry, and each iron atom is five-coordinate with square-pyramidal arrangements. Mössbauer spectra reveal the presence of high-spin iron(III) ions in complexes **1–4**. The magnetic susceptibility (300–2 K) indicate an antiferromagnetic interaction between the two oxygen-bridged iron(III) ions with $J = -17.5, -12.40, -19.0$ and -21.0 cm^{-1} for the complexes of **1–4**, respectively. The H₂O₂ disproportionation of complexes **1–4** in acetonitrile at 25°C show the rate law of $k_{\text{obs}}[\text{H}_2\text{O}_2]^2[\text{complex}]$. © 2001 Elsevier Science B.V. All rights reserved.

Keywords: Dimeric iron(III) complexes; Salicylaldehyde ligands; H₂O₂ disproportionation

1. Introduction

Functional models for a oxygen-bridged diiron(III) complex have received much attention [1–6]. They provide structural models for diiron sites in several proteins involved in oxygen storage of hemerytherin [7] and oxygen activation of methane monooxygenase [8]. Catalases catalyze the disproportionation of hydrogen peroxide to dioxygen and water, protecting cells against damage. Although most catalases contain the heme type iron(III)-protoporphyrin IX prosthetic group [9], recently, several synthetic oxo-bridged diiron(III) complexes showed catalase-like and oxygenation activity [10,11], in which it has been assumed that an active species may be an μ -oxo diiron(III) species for the catalase-like activity.

We have been particularly interested in alcoholic oxygen bridged binuclear iron(III) complexes as structural and functional models for catalases, and further to investigate the magneto-structural correlation. Herein we describe the preparation, structural characterization, magnetic properties, and H₂O₂ disproportionation activity of the diiron(III) complexes with the Schiff-base ligands which are obtained by condensing substituted salicylaldehyde with 3-amino-1-propanol.

2. Experimental

2.1. Preparations

All the chemicals used were of reagent grade and used as received. The ligands used in this study are Schiff-bases obtained by condensing the substituted salicylaldehydes, 5-bromosalicylaldehyde, 3-methoxysalicylaldehyde, 4-(diethylamino)-salicylaldehyde or 3,5-di-

* Corresponding author. Tel.: +886-2-262-15656, ext. 2531; fax: +886-2-262-28458.

E-mail address: tkwei@mail.tku.edu.tw (H.-H. Wei).

iodosalicylaldehyde with 3-amino-1-propanol in methanol; they are abbreviated as H_2L^1 , H_2L^2 , H_2L^3 , or H_2L^4 , respectively.

The complexes $[FeL^1Cl]_2$ (**1**), $[FeL^2]Cl_2$ (**2**), $[FeL^3Cl]_2$ (**3**), and $[FeL^4Cl]_2$ (**4**) were prepared in the same manner as follows [12]. To the ligand (10 mmol) was added a methanol solution (100 ml) of lithium methoxide (20 mmol); the resulting solution of the dianion of the ligands was added dropwise to a stirred methanol solution of $FeCl_3$ (1.621 g, 10 mmol). Upon heating the solution to reflux, a dark-red (**1**), violet (**2**), dark-green (**3**) or dark-red (**4**) crystalline product precipitated and was filtered off. The products were recrystallized from CH_3CN to give single crystals of complexes suitable for X-ray crystallographic analysis. *Anal. Calc.* for $C_{20}H_{20}Cl_2Br_2Fe_2N_2O_4$ (**1**): C, 34.57; H, 2.90; N, 4.03. Found: C, 34.80; H, 2.90, N, 3.76%. IR (KBr disc): $\nu(C=N)$, 1627(s), $\nu(Fe-O-Fe)$, 827 (w) cm^{-1} . *Anal. Calc.* for $C_{22}H_{26}Cl_2Fe_2N_2O_6$ (**2**): C, 44.26; H, 4.39; N, 4.69. Found: C, 43.97; H, 4.51; N, 4.33%. IR (KBr disc): $\nu(C=N)$ 1612(s); $\nu(Fe-O-Fe)$, 838 (w) cm^{-1} . *Anal. Calc.* for $C_{28}H_{40}Cl_2Fe_2N_4O_4$ (**3**): C, 49.51; H, 8.25; N, 5.94. Found: C, 48.95; H, 8.12; N, 5.74%. IR (KBr, disc): $\nu(C=N)$, 1585 (s); $\nu(Fe-O-Fe)$, 849 (w) cm^{-1} . *Anal. Calc.* for $C_{20}H_{18}Cl_2I_2Fe_2N_2O_4$ (**4**): C, 23.08; H, 1.74; N, 2.69. Found: C, 23.63; H, 1.80; N, 2.68%. IR (KBr, disc): $\nu(C=N)$, 1618(s); $\nu(Fe-O-Fe)$, 837 (w).

2.2. Physical measurements

IR spectra were recorded on a Bio-Rad FTS-40 FTIR spectrophotometer as KBr pellets in the 4000–

400 cm^{-1} region. UV–Vis absorption spectra were recorded on a Cintra 20 spectrophotometer. Mössbauer effect measurements were carried out using a ASA-600 spectrometer with $^{57}Co(Rh)$ source. All velocity scales and isomer shifts are referred to iron foil at 298 K. The temperature dependence of magnetic susceptibility was measured on a MPMS quantum design SQUID magnetometer in the range 2–300 K. Diamagnetic corrections were made using Pascal's constants [13].

2.3. X-ray crystal structure analysis

Crystallographic data were collected for compound **1** on an Enraf-Nonius CAD4 and for compounds **2–3** on a Siemens Smart CCD diffractometer with graphite-monochromatized Mo K_α radiation ($\lambda = 0.7107 \text{ \AA}$), $2\theta-\theta$ scan mode at 298 K. N independent reflections and N_o with $I > 2.0\sigma(I)$ were observed. The structures were solved by direct method and refined (based on F^2) by a full-matrix least-squares method using the SHELXTL software package [14]; the function minimized was $\sum w(|F_o| - |F_c|)^2$ and unit weights were used. All non-hydrogen atoms were readily located and refined with anisotropic thermal parameters; $R_1 = \sum |F_o - F_c| / \sum |F_o|$ and $wR_2 = (\sum w|F_o^2 - F_c^2|)^2 / \sum w|F_o^2|^{1/2}$. The summary of the crystal and diffraction data is given in Table 1 and selected bond distances and angles are given in Table 2.

2.4. Hydrogen peroxide decomposition

The H_2O_2 dismutation activity and turnover were carried out measuring the dioxygen evolution in acetonitrile with a complex: H_2O_2 ratio of 1:400. All reactions were carried out at 25°C in a 25 cm^3 reactor with stirring bar under air. Acetonitrile (15 cm^3) was added to the complex (25 μmol , 0.2 $mmol dm^{-3}$) and imidazole (20 mg) then the flask was closed with a rubber septum. Hydrogen peroxide (1 cm^3 , 30w/w (water) 10 mmol, 0.9 $mmol dm^{-3}$) was injected through the septum with a syringe. The reactor was connected to a graduated burette filled with water and dioxygen evolution was measured at time intervals of 10 s by volumetry. The turnovers of the reaction for the first 60 min for complexes **1–4** are 81, 60, 90 and 84, respectively. Observed initial rates were expressed as $mol dm^{-3} s^{-1}$ and calculated from the maximum slope of curves describing evolution of O_2 versus time, taking the volume of the solution into account. Plots of the initial rates versus the concentrations of H_2O_2 and iron(III) complexes **1–4** allowed determination of the reaction orders in both reactants. It should be noted that in the absence of imidazole the complexes were practically inactive towards peroxide.

Table 1
Crystallographic data for the complexes **1–3**

	1	2	3
Formula	$C_{20}H_{20}Br_2Cl_2Fe_2N_2O_4$	$C_{22}H_{26}Cl_2Fe_2N_2O_6$	$C_{28}H_{40}Cl_2Fe_2N_4O_4$
M	694.80	597.05	697.24
Space group	$P2_1/c$	$P2_1/n$	$P\bar{1}$
a (Å)	9.613(4)	8.1605(5)	7.4901(3)
b (Å)	14.606(5)	15.4836(9)	7.5182(3)
c (Å)	8.915(4)	10.5722(6)	14.3628(6)
α (°)			74.545(2)
β (°)	107.90(4)	111.498(1)	83.248(2)
γ (°)			86.448(2)
V (Å ³)	1191.2(8)	1242.90(13)	775.37(5)
Z	2	2	1
T (K)	295	296	296
D_{calc} ($Mg m^{-3}$)	1.937	1.595	1.455
N	2241	8705	6423
N_o	2095	2198	2708
R_1	0.0312	0.0527	0.0718
wR_2 (F^2)	0.0692	0.1138	0.1878

Table 2
Selected bond distances (Å) and bond angles (°)

Complex 1	Complex 2	Complex 3
<i>Bond lengths</i>		
Fe(1)–Cl(1)	Fe(1)–O(2)	Fe(1)–O(2)
2.2243(14)	1.864(3)	1.873(5)
Fe(1)–O(1a)	Fe(1)–O(1a)	Fe(1)–O(1a)
1.946(3)	1.974(3)	1.976(5)
Fe(1)–N(1)	Fe(1)–Cl(1)	Fe(1)–Cl(1)
2.060(3)	2.218(2)	2.240(2)
Fe(1)–O(1)	Fe(1)–O(1)	Fe(1)–O(1)
1.985(3)	1.959(3)	1.973(5)
Fe(1)–O(2)	Fe(1)–N(1)	Fe(1)–N(1)
1.894(3)	2.091(3)	2.065(6)
Fe(1a)–O(1)	Fe(1a)–O(1)	Fe(1a)–O(1)
1.946(3)	1.974(3)	1.976(5)
<i>Bond angles</i>		
O(1a)–Fe(1)–O(1)	O(2)–Fe(1)–O(1)	O(2)–Fe(1)–O(1a)
75.64(12)	145.6(2)	146.0(2)
O(1a)–Fe(1)–N(1)	O(1)–Fe(1)–O(1a)	O(1)–Fe(1)–O(1a)
142.44(13)	74.94(12)	74.9(2)
O(1)–Fe(1)–N(1)	O(1)–Fe(1)–N(1)	O(1)–Fe(1)–N(1)
88.43(13)	87.76(13)	86.9(2)
O(1a)–Fe(1)–Cl(1)	O(2)–Fe(1)–Cl(1)	O(2)–Fe(1)–Cl(1)
112.49(10)	107.76(12)	108.1(2)
N(1)–Fe(1)–Cl(1)	O(1a)–Fe(1)–Cl(1)	O(1a)–Fe(1)–Cl(1)
104.16(10)	109.37(10)	107.8(2)
O(2)–Fe(1)–N(1)	Fe(1)–O(1)–Fe(1a)	Fe(1)–O(1)–Fe(1a)
88.74(13)	105.06(12)	105.1(2)
O(2)–Fe(1)–O(1)	O(2)–Fe(1)–O(1a)	O(2)–Fe(1)–O(1a)
156.15(13)	90.60(13)	91.5(2)
O(2)–Fe(1)–Cl(1)	O(2)–Fe(1)–N(1)	O(2)–Fe(1)–N(1)
100.26(10)	88.49(14)	88.4(2)
O(1)–Fe(1)–Cl(1)	O(1a)–Fe(1)–N(1)	O(1a)–Fe(1)–N(1)
103.41(10)	147.38(13)	146.8(2)
Fe(1)–O(1)–Fe(1a)	O(1)–Fe(1)–Cl(1)	O(1)–Fe(1)–Cl(1)
104.36(12)	106.42(10)	105.7(2)
	N(1)–Fe(1)–Cl(1)	N(1)–Fe(1)–Cl(1)
	101.90(11)	103.7(2)

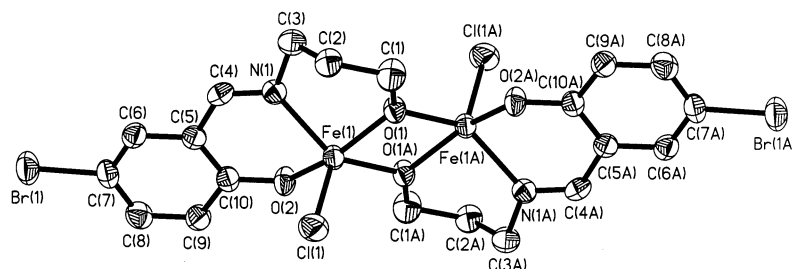


Fig. 1. Structure of $[\text{Fe}(\text{L}^1)\text{Cl}]_2$ (**1**) with the atom numbering scheme. Fifty percent probability ellipsoids are shown.

3. Results and discussion

3.1. Structure description

The structures and atom numbering schemes for complexes **1–3** are shown in Figs. 1–3, respectively, while selected bond lengths and angles are in Table 2. In all of the structures illustrated the coordination of the iron is square-pyramidal, with the donors of the tridentate ligand and the bridging alkoxide oxygen in the basal plane and the chlorine occupying the apical position of the square pyramid. The iron is displaced out of the basal plane towards the apical chlorine by 0.460 for **1**, 0.615 for **2** and -0.576 Å for **3**. The iron atoms of the dimer are bridged by the alkoxide oxygens to form a four-membered ring with iron–oxygen distances of 1.985(3) (Fe–O(1)), 1.946(3) (Fe–O(1A)) and 1.894(3) Å (Fe–O(2)) for **1**, 1.959(3), 1.974(3) and 1.864(3) Å for **2** and 1.973(5), 1.976(5) and 1.873(5) Å for **3**.

Studies of the Schiff-base iron(III) complexes have shown that the metal to imine nitrogen bond distance is sensitive to the electronic spin state of the metal ion: the

Fe–N(imine) distances are in the range ca. 2.00–2.10 Å for the high-spin state and in the range ca. 1.93–1.96 Å for the low-spin case [15]. In the structures of complexes **1–3** reported here the Fe–N bond distances of 2.060(3) for **1**, 2.091(3) for **2** and 2.065(6) Å for **3**, suggest that the iron(III) ions in **1–3** are in the high-spin state, which is consistent with the results of room temperature magnetic susceptibility and Mössbauer effect measurements (see below).

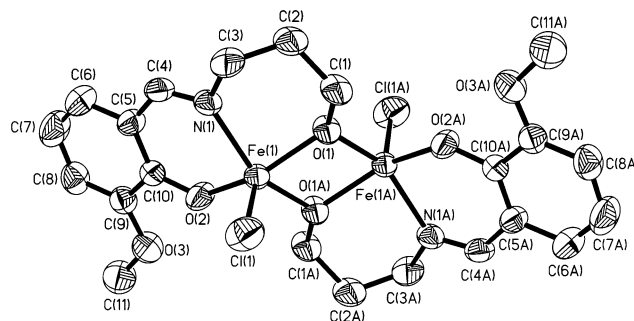


Fig. 2. Structure of $[\text{Fe}(\text{L}^2)\text{Cl}]_2$ (**2**). Details as in Fig. 1.

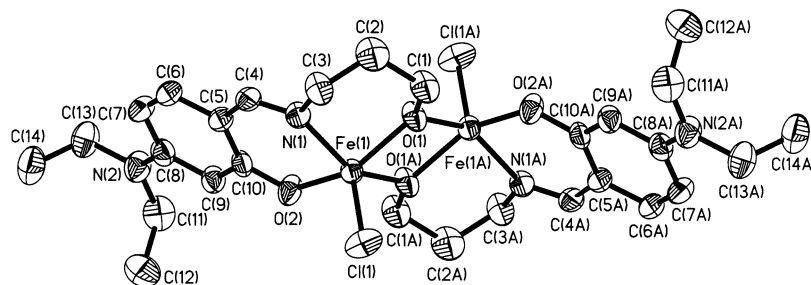


Fig. 3. Structure of $[\text{Fe}(\text{L}^3)\text{Cl}]_2$ (**3**). Details as in Fig. 1.

The Fe···Fe distance in **1** (3.105(3) Å), **2** (3.121(3) Å) and **3** (3.135(4) Å) increases as the Fe–O–Fe angle in **1** (104.36(12)°), **2** (105.06(12)°) and **3** (105.1(2)°) increases. The Fe···Fe distances in **1–3** are comparable to the Fe···Fe distances of 3.089 Å for $[\text{Fe}(\text{salpa})\text{Cl}]_2$ ($\text{H}_2\text{salpa} = N$ -(3-hydroxypropyl)(salicyaldimine)) [12] and 3.075–3.253 Å for $(\mu\text{-oxo})(\mu\text{-CH}_3\text{CO}_2)$ bridged dirron(III) complexes, while the Fe–O–Fe bond angles in **1–3** are similar to value of 104.1° for $[\text{Fe}(\text{salpa})\text{Cl}]_2$ and smaller than those of 128–120° for $(\mu\text{-oxo})(\mu\text{-CH}_3\text{CO}_2)$ -bridged diiron(III) complexes [10,11].

3.2. IR and electronic spectra

The IR spectra of complexes **1–4** shows bands at 827, 838, 849, and 837 cm^{-1} for complexes **1–4**, respectively, which may be assigned to the antisymmetric stretch of Fe–O–Fe [1,16]. The UV–vis spectra of the complexes **1–4** measured in acetonitrile reveal transitions at 324 and 459 nm for **1**, 335 and 497 nm for **2**, 346 and 433 nm for **3**, and 307 and 433 nm for **4**. The representative absorption spectra for **3** with and without imidazole added to the solution are shown in Fig. 4. The absorption bands at 433 and 346 nm may be assigned to phenolate–Fe(III) charge transfer transitions (LMCT) from p_π orbitals to d_{π^*} and d_{σ^*} , respectively [17,18]. In addition, it has been found that when imidazole was added there is no significantly change occurred in electronic spectrum of the solution after 30 min (see Fig. 4). It should be also noted here that the disproportionation of H_2O_2 in the acetonitrile solution by the complexes **1–3** caused drastic changes in the 433–497 nm region and the color of solutions changed to yellow, that is the disappearance of the LMCT bands (see insert in Fig. 4) indicating the dissociation of the phenolate–Fe(III) bond.

3.3. ESR and Mössbauer spectra and magnetic susceptibility

The powder X-band ESR spectra (9.80 GHz) at 298 and 78 K of all the complexes exhibit broad signals near $g = 2.0$ and 4.4 (very weak), with their relative intensities varying from complex to complex. The weak

signal near 4.4 corresponds to that predicted for a transition between the middle Kramers doublet of rhombically distorted, high-spin monomeric iron(III) impurities [12,19]. The signal found near $g = 2.0$ in the solid state may arise from a spin–spin coupled dimeric iron(III) species. The spectra of the complexes at room temperature and at 77 K differ only in the intensity of the high-field resonance, which decreases at low temperature due to depopulation of excited states.

The Mössbauer spectra of complexes **1–3** recorded at 295 K consist of a single quadrupole split doublet with the values of 0.90, 0.74 and 0.85 mm s^{-1} , and isomer shift (I.S.) values of 0.34, 0.37 and 0.39 mm s^{-1} , respectively. The representative spectrum of **3** is shown

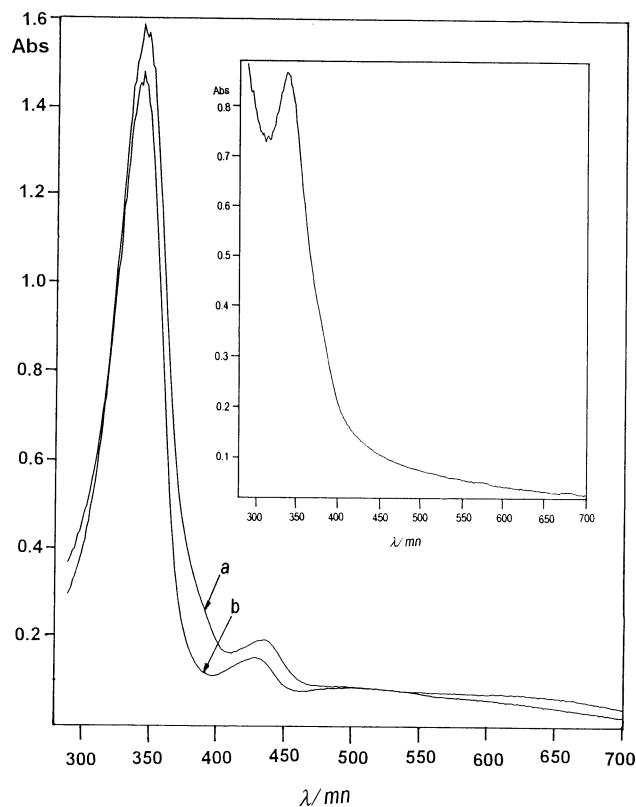


Fig. 4. UV–Vis spectra of complex **3** in acetonitrile solution (a) without imidazole and (b) 30 min after the addition of 2 equiv. of imidazole. Insert: the spectra recorded after the decomposition of H_2O_2 by complex **3** in imidazole added solution at 25°C.

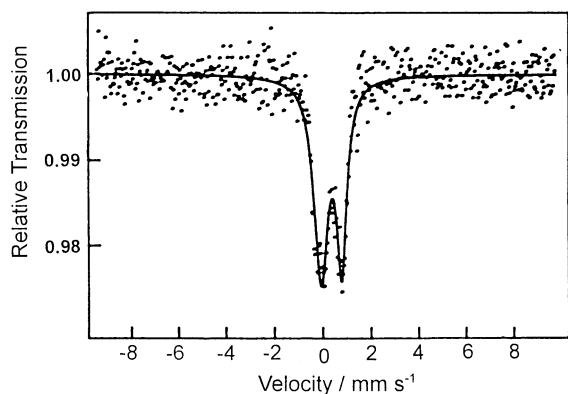


Fig. 5. Mössbauer spectra at 298 K of complex **3**. The solid line was plotted using the fitting parameters reported in the text.

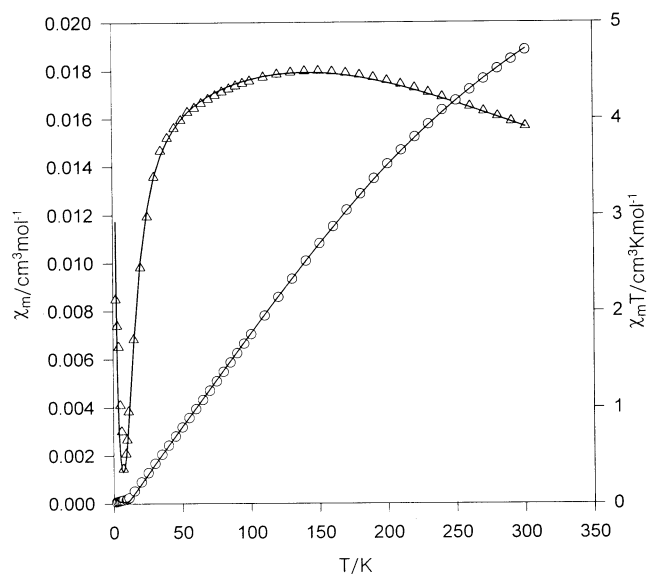


Fig. 6. Temperature dependence of χ_m (Δ) and $\chi_m T$ (\circ) for complex **3**. The solid lines represent the values are calculated with the parameters reported in the text.

in Fig. 5. The I.S. and Q.S. values for the three complexes indicate clearly the presence of high-spin iron(III) in a distorted five-coordination pyramidal ligand field [4,20–23].

Variable-temperature magnetic studies were performed on dried, powder samples of complexes **1–3** in the temperature range 2–300 K. Plots of χ_m and $\chi_m T$ versus T for **3** are shown in Fig. 6. The values of $\chi_m T$, 4.71 (300 K) and 0.02 $\text{cm}^3 \text{K mol}^{-1}$ (2 K) for **1**, 5.61 (300 K) and 0.18 $\text{cm}^3 \text{K mol}^{-1}$ (2 K) for **2**, 4.45 (300 K) and 0.02 $\text{cm}^3 \text{K mol}^{-1}$ (2 K) for **3** and 4.30 (300 K) and 0.12 $\text{cm}^3 \text{K mol}^{-1}$ (2 K) for **4**, indicate the operation of an antiferromagnetic interaction between the two high-spin iron(III) ions. The expression for the temperature-dependent magnetic susceptibility derived from the general isotropic exchange Hamiltonian ($H = -2JS_1 \cdot S_2$ for $S_1 = S_2 = 5/2$) is given by Eq. (1) [24]

$$\chi_m = (Ng^2\mu_B^2/kT)[A/B](1 - \rho) + 4.4\rho/kT \quad (1)$$

where $A = 2e^{2x} + 10e^{6x} + 28e^{12x} + 60e^{20x} + 110e^{30x}$, $B = 1 + 3e^{2x} + 5e^{6x} + 7e^{12x} + 9e^{20x} + 11e^{30x}$ and $x = J/kT$. The best least-squares fit was obtained and gave $J = -17.5 \text{ cm}^{-1}$, $\rho = 0.5\%$, $g = 2.0$ and $R = 4.0 \times 10^{-5}$ for **1**, $J = -15.4 \text{ cm}^{-1}$, $\rho = 2\%$, $g = 2.0$ and $R = 3.0 \times 10^{-5}$ for **2**, $J = -19.0 \text{ cm}^{-1}$, $\rho = 0.1\%$, $g = 1.98$ and $R = 2.8 \times 10^{-5}$ for **3**, $J = -21.0 \text{ cm}^{-1}$, $\rho = 0.2\%$, $g = 2.0$ and $R = 4.3 \times 10^{-5}$ for **4**, where R is discrepancy, defined as $R = (\chi_{\text{obs}} - \chi_{\text{calc}})^2 / (\sum \chi_{\text{obs}})^2$. The J values of 15.4–21.0 cm^{-1} measured for complexes **1–4** revealed insensitivity to the Fe–O–Fe bond angle and the Fe···Fe distance, and the values are in the range reported previously for non-heme (μ -alkoxo)- and (μ -hydroxo)diiron(III) complexes [1,12,18].

3.4. Studies of H_2O_2 disproportionation

The dependence of the initial rates of dioxygen evolution was examined with varying concentration of H_2O_2 and complexes **1–3**. In the first experiment, the hydrogen peroxide concentration was kept constant and the concentration of the complex was varied. Plots of the initial rate vs. catalyst concentration indicated that the reaction was first-order with respect to metal complex concentration. In a second experiment the catalyst concentration was kept constant and the H_2O_2 concentration was varied. The initial rate depends linearly on the square of the initial H_2O_2 concentration, as shown in Fig. 7. In the rate law (2) k_{obs} was calculated as 0.55 $\text{dm}^6 \text{mol}^{-2} \text{s}^{-1}$ for **1**, 0.54 $\text{dm}^6 \text{mol}^{-2} \text{s}^{-1}$ for **2**, 0.86 $\text{dm}^6 \text{mol}^{-2} \text{s}^{-1}$ for **3** and 0.40 $\text{dm}^6 \text{mol}^{-2} \text{s}^{-1}$ for **4**.

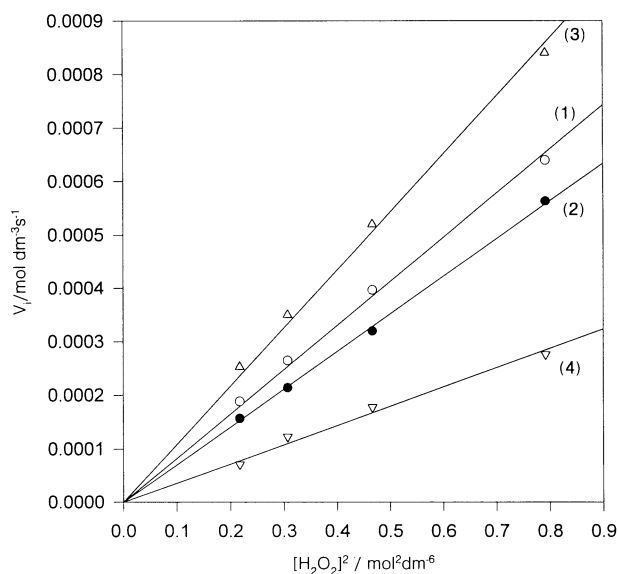


Fig. 7. Plots of the initial rate (V_i) of O_2 evolution as a function of $[\text{H}_2\text{O}_2]^2$ at 25°C and pH 7 in acetonitrile solution of complex **1** (\circ), **2** (\bullet), **3** (Δ) or **4** (∇).

Table 3

Comparisons of structural, magnetic and Mössbauer data and reaction rate of catalase-like reactions for complexes 1–3

	$\angle \text{Fe-O-Fe}$ (°)	$\text{Fe}\cdots\text{Fe}$ (Å)	J (cm^{-1})	I.S. (mm s^{-1}) ^a	Q.S. (mm s^{-1}) ^a	k ($\text{dm}^6 \text{mol}^{-2} \text{s}^{-1}$)	Ref.
$[\text{Fe}(\text{L}^1)\text{Cl}]_2$	104.36	3.105	−17.5	0.34	0.90	0.546	this work
$[\text{Fe}(\text{L}^2)\text{Cl}]_2$	105.06	3.121	−12.4	0.37	0.74	0.537	this work
$[\text{Fe}(\text{L}^3)\text{Cl}]_2$	105.10	3.135	−19.0	0.39	0.85	0.862	this work
$[\text{Fe}(\text{salpa})\text{Cl}]_2$ ^b	104.1	3.089	−17.0	0.33	1.00		[12]

^a Measured at 298 K.^b $\text{H}_2\text{salpa} = N$ -(3-Hydroxypropyl)salicyaldimine.

$$\text{rate} = k_{\text{obs}}[\text{H}_2\text{O}_2]^2[\text{complex}] \quad (2)$$

The results of kinetics studies of catalase-like model complexes 1–4 just described above are quite different from those of catalase-like hemerytherin model complexes with a $[\text{Fe}_2(\mu\text{-O})(\mu\text{-CH}_3\text{CO}_2)_2]^{2+}$ core [10,11] where the initial rate of the reaction was first-order with respect to $[\text{H}_2\text{O}_2]$ concentration. This implies that in the initial reaction, two H_2O_2 molecules individually attach to two iron(III) sites of complexes 1–4. At this stage, no actual catalytic mechanism is provided to interpret the present system, however, a possible catalytic cycle can be described as is known for the heme-type catalase [25–27].

In the heme catalases the peroxide reduction reaction $\text{H}_2\text{O}_2 + 2\text{e}^- + 2\text{H}^+ \rightarrow 2\text{H}_2\text{O}$ is accomplished by an Fe(III)–protoporphyrin IX center that generates compound **I**, formulated as a ferryl porphyrin π -cation radical ($\text{O} = \text{Fe}(\text{IV})^{\bullet+}$) [25–27]. This species catalyses the peroxide oxidation reaction $\text{H}_2\text{O}_2 \rightarrow \text{O}_2 + 2\text{e}^- + 2\text{H}^+$ in the case of heme peroxidases [26]. The observed stimulatory effects of electron-rich imidazole on H_2O_2 decomposition could be explained by its general acid–base catalytic properties, which would facilitate proton transfers, and favor homolysis of the O–O bond by reducing the activation energy [27]. For comparison some experimental data are listed in Table 3.

4. Supplementary material

Crystallographic data for the structural analysis have been deposited with the Cambridge Crystallographic Data Centre, CCDC no. 149087 for **2**, CCDC no. 149088 for **1** and CCDC no. 149089 for **3**. Copies of this information may be obtained from The Director, CCDC, 12 Union Road, Cambridge, CB2 1EZ, UK (fax: +44-1233-336033; e-mail: deposit@ccdc.cam.ac.uk or www: <http://www.ccdc.cam.ac.uk>).

Acknowledgements

This work is supported by grants from the National Science Council of Taiwan.

References

- [1] D.M. Kurtz, Jr, Chem. Rev. 90 (1990) 585.
- [2] L. Que, Jr, A.E. True, Prog. Inorg. 38 (1990) 97.
- [3] J.B. Vincent, G.L. Olivier-Lilley, B.A. Averill, Chem. Rev. 90 (1990) 1447.
- [4] A.L. Feig, S.J. Lippard, Chem. Rev. 94 (1994) 759.
- [5] U. Bossek, H. Hummel, T.W. Müller, E. Bill, K. Wieghardt, Angew. Chem. Int. Ed. Engl. 34 (1994) 2642.
- [6] B.J. Waller, J.D. Lipscom, Chem. Rev. 96 (1996) 2625.
- [7] (a) S. Sheriff, W.A. Hendrickson, J.L. Smith, J. Mol. Biol. 197 (1987) 273. (b) R.E. Stenkamp, L.C. Siekerand L.H. Jensen, J. Am. Chem. Soc. 106 (1994) 618.
- [8] (a) A.C. Rosenzweig, C.A. Fredrick, S.J. Lippard, P. Nordlund, Nature 366 (1993) 537. (b) A.C. Rosenzweig, P. Nordlund, P.M. Takahara, C.A. Fredrick, S.J. Lippard, J. Chem. Biol. 2 (1995) 409.
- [9] (a) I. Fita, A.M. Silva, M.R.N. Murthy, M.G. Rossmann, Acta. Crystallogr., Sect. B 42 (1986) 497. (b) I. Fita, M.G. Rossmann, J. Mol. Biol. 185 (1985) 21. (c) B.K. Vainshtein, W.R. Melik-Adamyanyan, V.V. Barynin, A.A. Vagin, A.I. Grebenko, V.V. Borisov, K.S. Bartels, I. Fita, M.G. Rossmann, J. Mol. Biol. 188 (1986) 49.
- [10] (a) B. Mauerer, J. Crane, J. Schuler, K. Wieghardt, B. Nuber, Angew. Chem. Int. Ed. Engl. 32 (1993) 289. (b) S. Ménage, J.M. Vincent, C. Lambeaux, M. Fontecave, J. Chem. Soc., Dalton Trans. (1996) 2081.
- [11] (a) S. Ito, T. Okuno, H. Matsushima, T. Tokii, Y. Nishida, J. Chem. Soc., Dalton Trans. (1996) 4479. (b) T. Okuno, S. Ito, S. Ohba, Y. Nishida, J. Chem. Soc., Dalton Trans. (1997) 3547. (c) S. Nishino, H. Hosomi, S. Ohba, H. Matsushima, T. Tokii, Y. Nishida, J. Chem. Soc., Dalton Trans. (1999) 1509.
- [12] (a) J.A. Bertrand, J.L. Breece, A.R. Kalyanaraman, J. Am. Chem. Soc. 92 (1970) 5233. (b) J.A. Bertrand, J.L. Breece, P.G. Eller, Inorg. Chem. 13 (1974) 125.
- [13] O. Kahn, Molecular Magnetism, VCH, New York, 1993, p. 3.
- [14] G.M. Sheldrick, SHELXL-93. Program for the Refinement of Crystal Structures, University of Göttingen, Germany, 1993.
- [15] (a) M. Calligaris, G. Nardin, L. Randaccio, Coord. Chem. Rev. 7 (1972) 385. (b) W.T. Oosterhuis, Struct. Bonding (Berlin). 20 (1974) 59.
- [16] K.S. Murray, Coord. Chem. Rev. 12 (1974) 1.
- [17] (a) R. Viswanathan, M. Palaniandavar, J. Chem. Soc., Dalton Trans. (1995) 1259. (b) R. Viswanathan, M. Palaniandavar, T. Balasubramanian, P.T. Muthiah, J. Chem. Soc., Dalton Trans. (1995) 2519. (c) R. Viswanathan, M. Palaniandavar, P. Prabhakaran, P.T. Muthiah, Inorg. Chem. 37 (1998) 3881.
- [18] A. Neves, L.M. Rossi, I. Vencato, W. Haase, R. Werner, J. Chem. Soc., Dalton Trans. (2000) 707.
- [19] (a) B. Chiari, O. Piovesana, T. Tarantelli, P.F. Zanazzi, Inorg. Chem. 21 (1982) 1396. (b) R.G. Wolman, D.N. Hendrickson, Inorg. Chem. 7 (1978) 45.

- [20] (a) K.S. Murray, *Coord. Chem. Rev.* 12 (1974) 1. (b) J.B. Vincent, G. Olivier-Lilley, B.A. Averil, *Chem. Rev.* 90 (1990) 1447.
- [21] C.C. Que, R.A. Lalancette, J.A. Potenza, H.J. Schugar, *J. Am. Chem. Soc.* 100 (1978) 2053.
- [22] B.J. Kennedy, K.S. Murray, P.R. Zwack, H. Homborg, W. Kalz, *Inorg. Chem.* 14 (1985) 3302.
- [23] R. Hotzelmann, K. Wiegardt, J. Ensling, H. Romstedt, P. Gütlich, E. Bill, U. Flörke, H.J. Haupt, *J. Am. Chem. Soc.* 114 (1992) 9470.
- [24] C.J. O'Connor, *Prog. Inorg. Chem.* 29 (1982) 203.
- [25] D.T. Sawyer, *Oxygen Chemistry*, Oxford University Press, New York, 1991, p. 21.
- [26] K.Y. Xie, D. Dolphin, in: G. Berthon (Ed.), *Handbook of Metal–Ligand Interactions in Biological Fluids*, Marcel Dekker, New York, 1995, pp. 339–351.
- [27] (a) J.H. Dawson, *Science* 240 (1988) 433. (b) M. Sono, M.P. Roach, E.D. Coulter, H. Dawson, *Chem. Rev.* 96 (1996) 2841.